International Journal of Advanced Science and Research
ISSN: 2455-4227
Impact Factor: RJIF 5.12
www.allsciencejournal.com
Volume 2; Issue 6; November 2017; Page No. 01-07

Photocatalytic activity of α-Phase bismuth oxide nanoparticles under visible light

[*1] G Viruthagiri, [2] P Kannan, [3] VK Indhumathi
[1] Department of Physics, Annamalai University, Annanmalainagar, Tamil Nadu, India
[2] Department of Physics, R&D center, Bharathiar University, Coimbatore, Tamil Nadu, India
[3] Department of Physics, Sri Vidya Mandir Arts and Science College, Uthangarai, Krishnagiri, Tamil Nadu, India

Abstract
α-phase bismuth oxide nanoparticles successfully prepared by precipitation method and characterized with thermo gravimetric analysis and differential thermal analysis, X-ray diffraction, Photo luminance, Field emission scanning electron microscope, Energy dispersive X-ray diffraction FT-IR spectra and UV-Vis diffuse reflectance spectroscopy. The bismuth oxide particles annealed at 500 °C exhibited α-phase. Photocatalytic experiments indicated that the obtained Bi_2O_3 nanoparticles were highly active for photodegratation of methline blue.

Keywords: bismuth oxide, photocatalytic, irradiation, phase changes

1. Introduction
Bismuth oxide (Bi_2O_3) has received considerable attention over last three decades. It is well known that bismuth oxide has six polymorphic forms, denoted by Bismuth oxide α-Bi_2O_3 (monoclinic), β-Bi_2O_3 (tetragonal), δ-Bi_2O_3 (face centered cubic) [1] γ-Bi_2O_3 (body centered cubic) ϕ-Bi_2O_3 (orthorhombic) [2] and Bi_2O_3 (triclinic) respectively. Among them, the low temperature α-phase and the high temperature δ-phase are stable, but the others are high temperature metastable phase What's more, it has a lot of peculiar physical and chemical properties, such as a wide energy gap change (from 2 to 3.96 eV) [3] high oxide ion conductivity properties (1.0 s/cm) [4], high refractive index, dielectric permittivity, besides excellent photo conductivities and photoluminescence Due to its peculiar properties, bismuth oxide has become one of the important functional materials which have been applied in a wide range of areas, such as solid oxide fuel cells, gas sensors, photo catalyst, energetic materials and others. For the above mentioned applications, crystal forms, particle structure and size and specific surface area are very important. Among various semiconductors a p-type Bi_2O_3 heterogeneous semiconductor was considered as one of the most efficient photo catalyst and important in modern solid state due to its unique structure and physical attribute like high refractive index and high thermal stability, produce highly reactive species for initiating oxidation reaction for degradation of dyes, gases and dyes chemistry [5]. Among all phases the band gap of the low temperature α-phase is (2.8eV) and therefore found to be active in the visible region. Recently, bismuth oxide have been synthesized through different methods, such as co-precipitation, Solgel method chemical vapour deposition microwave-assisted method [6]. Chemical precipitation synthesized powders offer many advantages, such as high degree of crystalline, well controlled morphology, high purity and narrow particle size distribution, using $Bi(NO_3)_3.5H_2O$ as raw materials [7-8]. In the present work, precursors of Bi_2O_3 were synthesized through simple chemical precipitation method using bismuth nitrate and diluted (1:8%) nitric acid, sodium hydroxide. The synthesized precursors of Bi_2O_3 were analyzed by TG-DTA to get values of temperature at which the precursors decompose into bismuth oxide.
After proper calcinations, the obtained pure powders of α-Bi_2O_3 were characterized by techniques like XRD, FTIR, PL, FE-SEM, and TEM and photocatalytic activity.

2. Experimental
2.1 synthesis of bismuth oxide nanoparticles
In the chemical precipitation method, the stoichiometric ratios of the materials Bismuth Nitrate Penta Hydrate ($Bi_2(NO_3)_2.5H_2O$), Sodium Hydroxide (NaOH), was used as a precursors. All chemicals were used as received in analytical reagent (AR) grade. For Bi_2O_3, 1.0M of Bismuth Nitrate Penta Hydrate was dissolved in 50 ml of deionized water and then stirred the solution vigorously. Then, 0.1M of Sodium Hydroxide dissolved in 50 ml of deionized water was added drop wise to the above solution under stirring. The mixed solution was heated at 80 °C and continuously stirred for 4 h. A light yellow precipitate was formed. Then, the obtained precipitate was washed repeatedly with deionized water and then filtered. The precipitate was dried in hot air oven at 100 °C for 1 h, and then the product was annealed at 500 °C in muffle furnace for 4 h to get Bismuth Oxide nanoparticles.

3. Results and Discussion
3.1 Thermal analysis measurement
Thermal analyses of the synthesized nanoparticles were done by using TGA and DTA. The TGA and DTA analysis was carried out under nitrogen atmosphere. TGA analysis showed that they were three serious of weight loss in the TGA analysis of pure Bi_2O_3 nano particles. Fig. 1 shows the TGA and DTA

curves of pure Bi_2O_3 nano particles. Region first from 55ºC – 220ºC which was due to the evaporation of the physical water adsorbed at the surface of the powder, and the region second from 220- 512º C, caused by the removal of lattice waters O-H [7]. Finally little change in the TG curve can be observed after 512 ºC, which reveals that the decomposition of the nitrate species to yield bismuth oxide only at 500 ºC as the calcinations temperature is remarkably lower than that used in the traditional precipitation method. The weight loss from pure Bi_2O_3 at midpoint (175ºC, 512ºC, 900ºC) was found to 0.79, 3.74 and 4.27% respectively. The DTA curve exhibits an exothermic peaks at around 220 ºC which was must be considered a weight loss as physically and chemically observed molecular water and hydroxyl groups [9]. The second region corresponds to a slight weight loss 500ºC up to roughly 760ºC due to the decomposition of traces hydroxides, which leads to a progressive shrinkage of materials due to crystallizations to the residual amorphous phase,The endothermic peaks at 307 ºC and 862 ºC correspond to decomposition of some residual organic species. To study the thermal behavior of the prepared $Bi_2(OH)_3$ and bismuth nitrous Bi_2NO_3. TG/DTA was performed simultaneously in the temperature 30 – 900 ºC as shown in the (Fig. 1) the thermal decomposition $2Bi(NO_3)_3$ occur in two major steps. Step one the removal of surface at adsorbed water associated with the $2BiNO_3$ (55-220ºC) and step two the decomposition of bismuth nitrate into bismuth oxhydroxide into α-bismuth oxide (220-520ºC). After ~ 500ºC, weight loss completely ceased as a consequence, a stable residue can be ascribed to α-bismuth oxide nanoparticles [10].

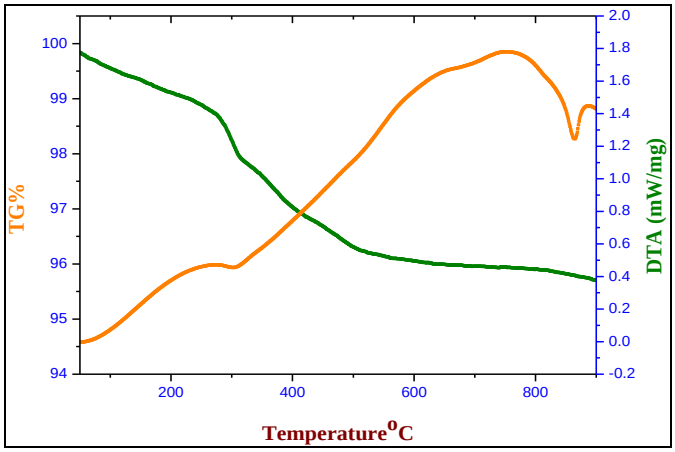

Fig 1: TG and DTA curve of synthesized bismuth oxide nanoparticles

The dehydration involved in the first stage is given by the following chemical reaction

$Bi_2(NO_3)_2.5H_2O + 2HNO_3 \rightarrow 2Bi(NO_3)_3 + 6H_2O$ -------- (1)

$Bi_2(NO_3) + 6NaOH \rightarrow 2Bi(OH)_3 + 6NaNO_3$ -------- (2)

$2Bi(OH)_3 \rightarrow Bi_2O_3 + 3H_2O$ -------- (3)

$Bi_2O_3 \xrightarrow[\Delta]{500ºC} \alpha\text{- } Bi_2O_3$ -------- (4)

As per the available literature [10] the water content for $2Bi(OH)_3$ varies from 0-0.79% and for $2Bi(OH)_3$, it varies from 0.79-3.74% TG and DTA curves of bismuth oxyhydroxide $2Bi(OH)_3$ prepared using bismuth nitrate pentahydrate $Bi_2(NO_3)_2.5H_2O$ and dilute 1% nitric acid as shown Fig.1, the TG curve shows two major weight losses. The initial weight loss between room temperature and 220ºC is attributed to the loss of 2 or 3 water molecules from bismuth oxyhydroxides. The second major weight loss in the range of 220-500ºC is due conversion of unstable bismuth oxide (at~ 300ºC) to α- Bi_2O_3. After these fragments at temperature up to 900ºC, no thermal effects are observed in the TG curve indications the formation of pure bismuth oxide nanoparticles. The formation of α- Bi_2O_3 illustrated by the above given equations (1-4).

3.2 X-Ray powder diffractions

The crystallographic information's of as prepared bismuth oxide nano particles were corroborated by X ray diffraction pattern (Fig.2). Three characteristic peaks are indexed as (120), (200) and (121),indicating that monoclinic Bi_2O_3 (JCPDS-71-0465), P21/C(14) has come into being the XRD results demonstrate that there are no impurities existing in powders [11].

According to the JCPDS card, the synthesized product is a monoclinic phase with cell parameters of a = 5.850, b=8.165, and c= 5.130Å and β= 112.38° and space group of P21/ C (14).

The average size of α- Bi_2O_3 crystallite (54nm) were calculated using Scherer's formula.

$$D = k\lambda/\beta\cos\theta \text{----------(1)}$$

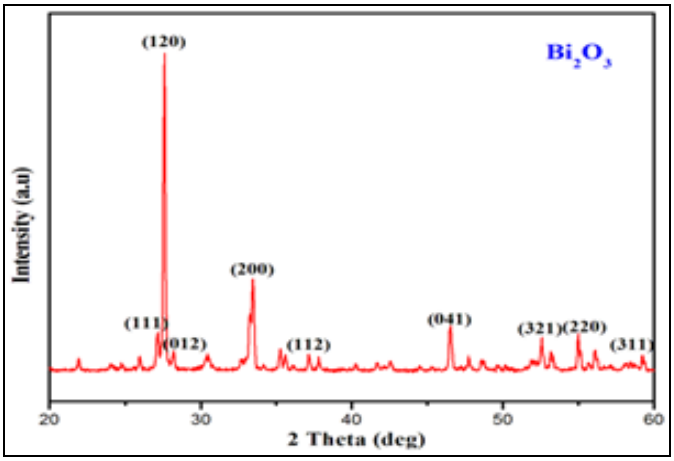

Fig 2: X-Ray powder diffratogram of synthesized α- Bi_2O_3nano particle

Where, D is the crystallite size, K is the shape factor, λ is the wave length of X-ray sources (0.154nm), β is the full width at half maximum, θ is the diffraction angle. The absence of impurities peaks indicates that unstable α- Bi_2O_3 crystallite (at 300 ºC) and unstable β-- Bi_2O_3 (up to 420ºC) are completely decomposed into α- Bi_2O_3 at 500 ºC. The bigger crystallite size of α -Bi_2O_3 suggests it's less or narrow width of the XRD characteristics peaks.

3.3 UV-Vis Diffuse Reflectance spectra (UV-DRS)

The Optical properties of α-Bi_2O_3 nanoparticles were

scrutinized by UV-Vis-DRS spectrometers. The different phase composition also had significant effect on the optical absorption properties of Bi_2O_3 which was confirmed by DRS the room temperature absorption spectrum of pure α-Bi_2O_3 nanoparticles in the wavelength region of 300 to 700nm. The band gap (E_g) of pure α-Bi_2O_3 was defined from the wavelength value corresponding to the intercept point of the straight line at a = 0 and E_g value is calculated by using equation (2).

$$E_g = \frac{hc}{\lambda} eV \text{ (or)}$$

$$E_g = \frac{1240}{\lambda} eV \text{ ---------- (2)}$$

Where, E_g is the band gap energy(eV), h is the Planck's constant ($6.626x10^{-34}$ JS), C is the light velocity ($3x10^8$m/s) and λ is the wavelength (nm). The calculated band gap energy E_g of α- Bi_2O_3 was found to be 2.64eV.

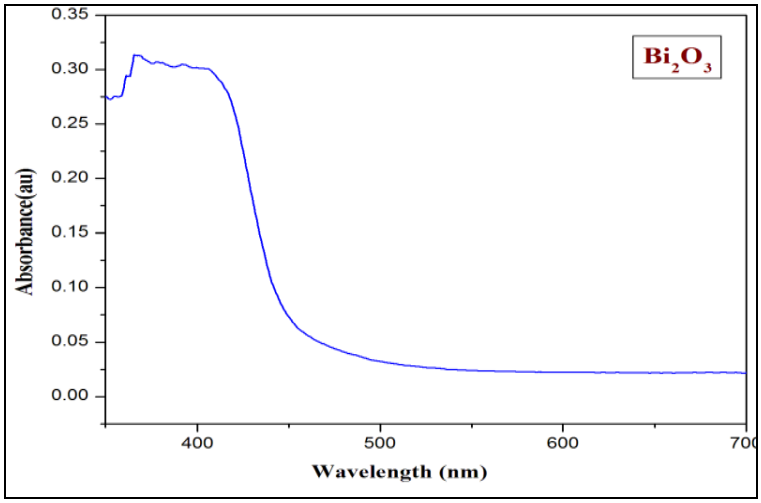

Fig 3: UV-Vis Diffuse Reflectance spectrum of synthesized α- Bi_2O_3 nano particles

According to the spectrum (Fig.3) the as prepared nano particles present the photo absorption properties from UV light region to visible light shorter than 470 nm, which is assigned to the intrinsic band gap absorption. There is no absorption peak after ≈ 450 nm for the Bi_2O_3 calcined at 500ºC is probably caused by purity of the sample [12]. The higher the band gap of bismuth oxide (3.2eV) than as prepared α-Bi_2O_3 (2.64eV) for annealed at 500ºCmay be due to the inclusion of hydroxide. However, after annealing the band gap is decreased to 2.77eV [12]. The decrease in band gap after annealing is a consequence of phase change to monoclinic Bi_2O_3. The result further confirms that the powder XRD technique is α -Bi_2O_3 typical monoclinic structure.

3.4 Photoluminescence (PL) analysis

Figure.4 shows the optical absorption spectrum of α-Bi_2O_3 nanoparticles.The maximum at 467nm is assigned to the optical transmission of the first excitation state. The obvious blue shift of the absorption peak relative to bulk bismuth may be attributed to the quantum-confinement effect of α-Bi_2O_3 nanoparticles. The visible emission is recognized from the radiative recombination of photo generated hole with an electron occupying the bismuth and oxygen vacancies [13].

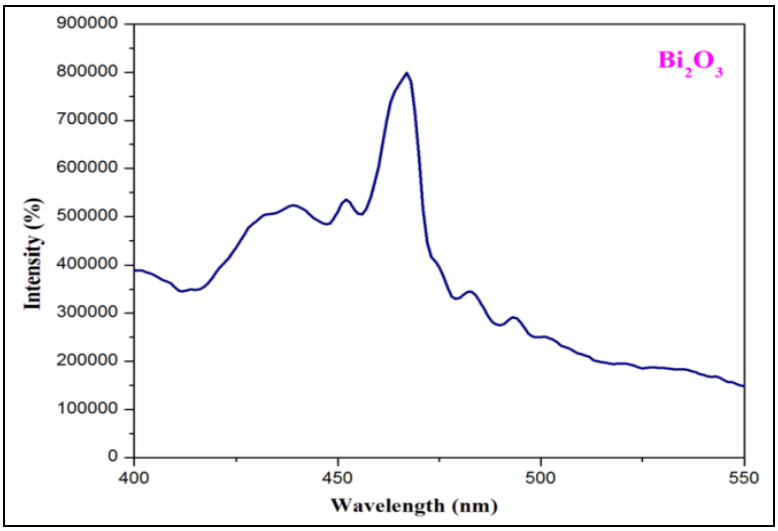

Fig 4: Photoluminescence of synthesized α- Bi_2O_3 nanoparticles

Photoluminescence spectrum analysis is a powerful technique to survey the separation efficiency of the photo generated electron - hole pair in a semiconductor. The emission peak around 467 nm appears for α-Bi_2O_3, which may be derived from the direct electron - hole recombination of band transition. The efficient charge separation could increase the life time of charge carriers are enhancing the efficiency of interfacial charge transfer to adsorbed substrates, and then improve the photo catalytic activity.

3.5 Functional group analysis (FTIR)

FTIR analysis has been recorded for the (prepared) annealed sample in the range of 400-4000 cm^{-1} and the result is shown in Fig.5.In the FTIR spectrum of α-Bi_2O_3, the peak at 540 cm^{-1} is assigned to the Bi-O-Bi stretching vibration and the peak around 620 cm^{-1}can be attributed to the Bi-O stretching vibration of non-bonding oxygen of the distorted Bi-O polyhedral [14].

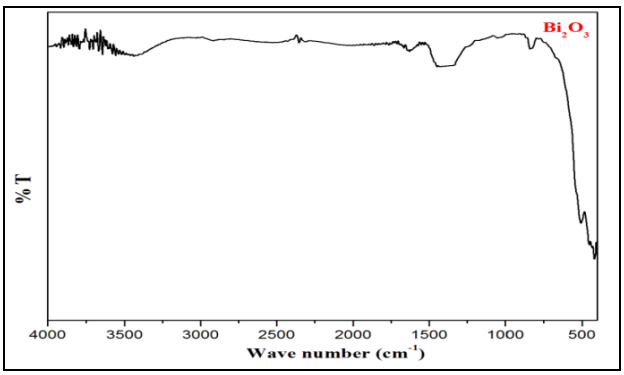

Fig 5: FTIR spectrum of synthesized of α- Bi_2O_3

The peakaround 840cm^{-1}has been assigned to Bi-O monoclinic phase of the octahedral Bi_2O_3 nanoparticles. The intense band at 1350 – 1390cm^{-1} possibly arises due to stretchingvibrations of the NO_3 ion the medium and broad peak at 1600 - 1640 cm^{-1} is due to the bending vibration of the absorbed water, and the peaks at 3300-3500 cm^{-1}here attributed to the stretching vibration of observed hydroxyl functional groups, which is believed that these groups came from the hydrolysis in the chemical synthesis process From the IR spectrum of prepared sample (α-Bi_2O_3) Fig. 5, the intensities of starching and bending vibration bonds of water molecules have been reduced considerably indicating the high purity of the product. The absorption bands located at ≈1380 and 840 cm^{-1} are due to the NO_3^{2-} anions [15]. Further, no absorption bands of anions were predicted in sample α-Bi_2O_3 indicating proper formation of crystalline α-Bi_2O_3.

3.6 FE SEM

The microstructure analysis of the sample (α-Bi_2O_3) was carried out by FE-SEM analysis. A review of reference literature showed that researchers have been less focused on the particle morphology of Bi_2O_3 polymorphs although this is crucial in the applications of Bi_2O_3 powders. For that reason, we focused more on this problem by using high-resolution scanning electron microscopy Fig. 6(a& b) shows. FE-SEM micrographs of the α-$Bi_2O_3$the micrographs of the α-Bi_2O_3 as prepared material at different magnifications showed Fig. 6(a & b) that the α-Bi_2O_3 has highly compact needle or rod like structure with sharp edges [16]. High resolution images revealed that individual needle was composed by a collection of elongated particles. The α-Bi_2O_3 particles were of almost identical widths Fig. 6(b).

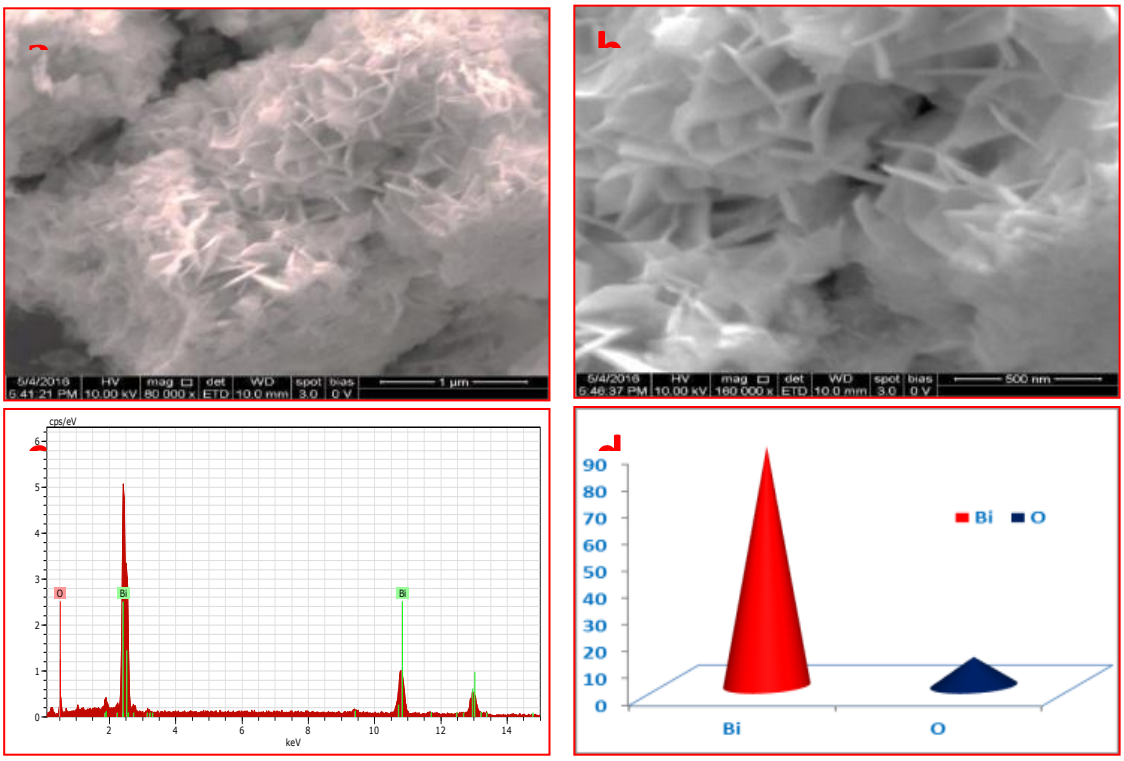

Fig 6(a & b): FE-SEM image of undoped Bismuth Oxide nanoparticles, and **6(c & d):** EDX and percentage of elements of Bismuth Oxide nanoparticles

The presence of a low fraction of small-sized α-Bi_2O_3 particles is also visible in the same micrographs [17]. These differences show a very high dependence of α-Bi_2O_3 microstructure on the synthesis route. BiOOH particles (Fig. 6(a & b)) exhibit a cloverleaf morphology (Fig. 6(b)). The micrograph of the cross-section of one particle Fig.6(a) show that these particles possess a substructure that is, they are made up of much smaller primary BiOOH particles. It can also be noticed that BiOOH particles are so arranged that the width of the secondary particle has almost the same value at different surface points.The EDX results of the α-Bi_2O_3 nanoparticles have been depicted in Fig.6(c).The result shows the presence of Oxygen (O) and Bismuth (Bi) are the only elements according to weight percentage of 10.17% and 89.83% respectively. For morphological confirmations, TEM images were recorded for α-Bi_2O_3.

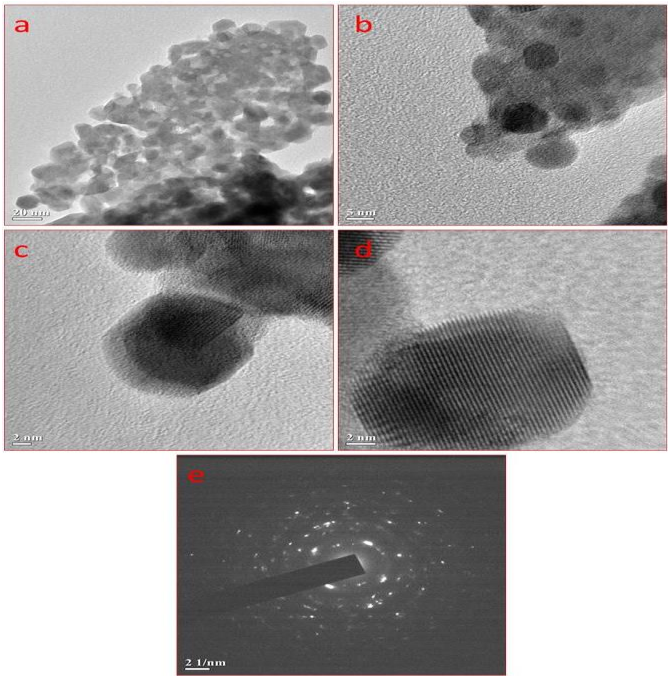

Fig 7(a-e): HR-TEM images of different magnification range of Bismuth Oxide nanoparticles, (e) SAED pattern of Bismuth Oxide nanoparticles

Figures 7(a&b) shows the aggregated nanoparticles, investigated by TEM. Combine with the HR-TEM images Fig.7(c&d) show that the continuous lattice fringes, this image clearly displays that the lattice fringes of as synthesized α-Bi_2O_3 have no defect appearance. It can be seen from Fig.7 (e) that the selected area electronic diffraction (SAED) pattern of α-Bi_2O_3 nanoparticles showed typical monoclinic structure [18].

The lattice distances calculated from the diffraction rings in Fig.7 (e) is 3.25 Å (120) (characteristic peak) [18]. This distance coincide with those of the XRD data in JCPDS No.71-0465, which is the standard XRD data of bulk α-Bi_2O_3.Therefore the Bi_2O_3 nanoparticles was identified to be α-Bi_2O_3, which belongs to monoclinic system with P21/c(14) space group. Electron diffraction patterns Fig.7 (e) showed the brightness and intensities of polymorphic discrete ring of the crystalline nanoparticles.

3.7 UV absorption and photo catalytic activity of α-Bi_2O_3 nanoparticles

The photo catalytic activity of α-Bi_2O_3 nanoparticles was investigated using degradation of aqueous methylene blue (MB) dye solution. Fig.8 shows the absorption spectra of methylene blue (MB) dye using α-Bi_2O_3 catalyst as a function of wavelength (400-800 nm) for various time intervals (0, 15,30, 45, 60, 75, 90, 105, 120 and 135 min). The degradation effect was characterized by monitoring the absorption peak of methylene blue dye centered at 664nm. The plots clearly demonstrate that the prepared α-Bi_2O_3nanopowders easily degrade the methylene blue dye with slight increase of time. From the Fig.8we can say that the maximum absorption peak (at 664nm) decreases with increasing irradiation time. This illustrates that the methylene blue dye concentration decreases in the presence of α-Bi_2O_3 catalyst and solar light illumination. The decrease in the absorption of the mixed solution was due to the distraction of the homo and hetro-poly aromatic rings present in the dye molecules or due to rapid degradation of methylene blue (MB), which is confirmed by the lower intensities of the absorbance peak of methylene blue (MB).

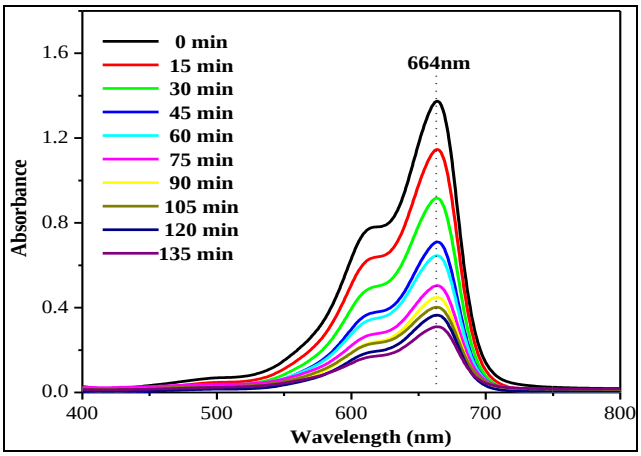

Fig 8: Absorbance spectra changes of Methylene Blue solution after different irradiation times of as synthesized undopedBi_2O_3 nano particles

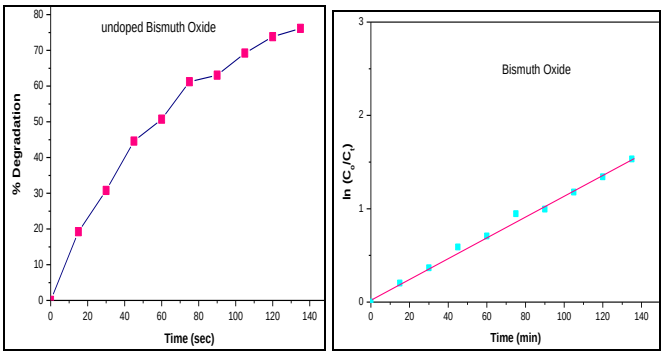

Fig 9(a&b): Change in kinetic energy of Methylene Blue solution after different irradiation times of as synthesized undoped Bi_2O_3 nanoparticles

The effect of α-Bi_2O_3 on percentage degradation of the methylene blue (MB) dye has been examined by varying the time interval from 0-135 min and the results are presented in

Table 1: Change in kinetic energy of MB solution after different irradiation times of as synthesized undoped Bi_2O_3 nanoparticles

Time (min)	0	15	30	45	60	75	90	105	120	135
α - Bi_2O_3	0	19.23	30.76	44.61	50.76	61.23	63.07	69.23	73.84	76015

The percentage degradation increase rapidly with the increase in the time for methylene blue (MB) (α-Bi_2O_3) solution. The maximum degradation of methylene blue (MB) dye took place in 135 min of irradiation with sunlight using α-Bi_2O_3 catalyst was 76.15%. Generally the photocatalytic activity of semiconductor photocatalyst not only depends on their electronic structure as well as depends on many other factors such as morphology, surface area and crystalline phase and size [19]. It is obvious that the higher surface area with larger pores play an active role in the absorption of substance, which results in the higher photocatalytic activity. The higher surface area also provides a higher number of catalytic sites on the surface of α-Bi_2O_3 with less recombination of electron hole pairs, which is the rate determining step in the photocatalytic degradation Figs.9(b&c).The optimum band gab also plays an important role in the photocatalytic activity of α-Bismuth oxide. Electron hole pair generation is dependent on the band gap of α-Bi_2O_3, the increase in the band gap is useful to obtain higher electron hole pair generation.

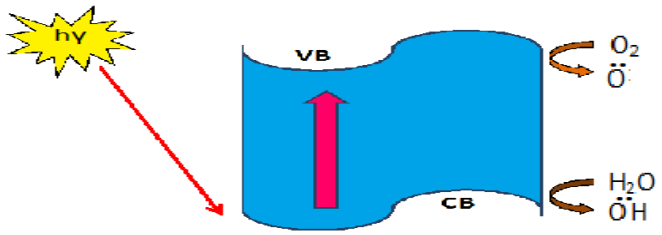

Fig 9(c): General mechanism for the degradation of dyes

Subsequently, the departed electrons and holes migrate to the surface of the catalysts and react with adsorbed O_2 and H_2O respectively, forming O_2 and OH, the man species (equations of reactions) responsible for the degradation of pollutants, such as methylene blue (MB) in the present case. The degradation time, dye concentration and degradation percentage reveals (Fig.8) that the α-Bi_2O_3 nanoparticles which characteristics and dimensions as described above can be used as a future photocatalyst. The reason for the efficient photocatalyst can be accounted to the small volume of the nanoparticles, good crystallinity and presence of oxygen defect in the crystal structure.

4. Conclusion

In summary, we report a simple chemical precipitation route for the fabrication of α-Bi_2O_3 nanoparticles. The XRD pattern indicated the monoclinic α-Bi_2O_3. The size of the obtained particles was in the range of 54nm, as confirmed from the Debye Scherer's equation and observed with transmission electron microscopy (TEM). The FE-SEM images clearly displayed the formation of needle or rod like morphology. The TGA and DTA results showed different decomposition patterns of the Bismuth Oxide. The as prepared α-Bi_2O_3 indicate the good photo catalytic decomposition and hence reduced in the electron-hole recombination and extended spectral response to the visible region inferred from the UV-visible absorption spectrum. It is concluded that the crystallite size plays an important role in deciding the performance of the catalyst.

5. References

1. Fritz DM, *et al.* Solids Interatomic Potential with X-rays Ultrafast Bond Softening in Bismuth Mapping Science. 2007; 315:633.
2. Cornei N, Tancet N, Abraham F, Mentré O. Synthesis and characterization of Bismuth oxide nanoparticles via sol-gel method *Inorganic Chemistry*. 2006; 03(04):162-165.
3. Leontie L, Caraman M, Alexe M, Harnagea C. Structural and optical characteristics of bismuth oxide thin films, *Surf. Sci.* 2002; 507:480-485.
4. Sammes NM, Tompsett GA, Naafe H, Aldinger F. Bismuth based electrolytes structure and ionic conductivity J Euro. Ceram. Soc. 1999; 19:1801-26.
5. Fan HT, Teng XM, Pan SS, Ye C, Li GH, Zhang LD. Optical properties of δ-Bi_2O_3 thin films grown by reactivesputtering, *Appl. Phys. Lett.* 2005; 87:15-222.
6. Patil MM, Deshpande VV, Dhage SR, Ravi V, Synthesis of Bismuth Oxide Nanoparticles at 100 °C, *Matterial letters.* 2005; 59(19-20):2523-2525.
7. Yamashita H, Harada M, Misaka J, Takeuchi M, Neppolian B, Anpo M. Photocatalytic degradation organic compound diluted in water using visible light responsive metal ion implanted TiO_2, *Catal. Today.* 2003; 84:191-196.
8. Kim H, Kim J, Kim W, Choi W. Enhanced photocatalytic and photoelectrochemical activity in the ternary hybrid of CdS/TiO_2/WO_3 through the cascadal electron transfer J Phy. Chem. 2011; 115(19):9797-9805.
9. Simon S, Eniu D. Spectroscopic characterisation of local structure in Y_2O_3-B_2O_3-Bi_2O_3 glasses doped with gadolinium, J Mater. Sci. 2007; 42:5949-5953.
10. Clark IJ, Takeuchi T, Ohtori N, Sinclair DC. Hydrothermal synthesis and dielectric properties of tetragonal $BaTiO_3$, J. Mater. Chem. 1999; 9:83-91.
11. Iyyapushpam S, Nishanthi ST, Pathinettam Padiyan D. *Materials Letters.* 2012; 86:25-27.
12. Marijangotic, StankoPopovic, Svetozar Music. *Materials Letters.* 2007; 61:709-714.
13. Kumari LN, Li WZ, Vannoy CH, Leblanc RM. Vertically aligned and interconnected nickel oxide nanowalls fabricated by hydrothermal route, Crystal Reseach and technology. 2009; 44:495-498.
14. Dimitriev Y, KrupchanskaIvanova MY, Staneva A. Sol-Gel Synthesis of material in the system Bi_2O_3-SiO_2, J Chem. Techn. Met. 2010; 45:39-42.
15. Fu H, Pan C, Yao W, Zhu Y. Visible light induced degradation of Rhodamine B by nanosized BiZWOG, J Phys. Chem. B. 2005; 109:22432-22439.
16. Wenting Dong, Congshan Zhu. Optical properties of surface modified Bi_2O_3nanoparticles, Journal of physics

and chemistry of solids. 2003; 64:265-271.
17. XIA Ji-yong, TANG Mo-tang, CHEN Cui. JIN Sheng – ming. CHEN Yong-ming., Preparation of α- Bi_2O_3 from powders through low temperature oxidation, Transactions of Nonferrous metals, Society of china. 2012; 22:2289-2294.
18. Raza W, Haque MM, Muneer M, Synthesis of visible light driven ZnO characterization and photocatalytic performance, Appl. Surf. Sci. 2014; 322:215-224.
19. Li K, Yang C, Xu Y, Ying D, Wang Y, Jia J. Effect of inorganic anions on rhodamine B removal under visible light irradiation using Bi_2O_3/Ti rotating disk reactor. Chem. Eng. J. 2013, 211-212:208-215.